

Real-time Traffic Simulation and Management for Large-scale Urban Air Mobility: Integrating Route Guidance and Collision Avoidance

Canqiang Weng^{a,1}, Can Chen^{a,b,1}, Jingjun Tan^a, Tianlu Pan^c, Renxin Zhong^{a,*}

^a*School of Intelligent Systems Engineering, Sun Yat-Sen University, Shenzhen, China*

^b*Department of Civil and Environmental Engineering, The Hong Kong Polytechnic University, Hong Kong, China*

^c*Department of Network Intelligence, Peng Cheng Laboratory, Shenzhen, China*

Abstract

With a vision to expand the transport supply using low-altitude airspace, urban air mobility (UAM) has emerged as a promising alternative to provide point-to-point travel in congested areas. The rapid development of electric vertical take-off and landing vehicles will promote UAM as a viable and sustainable transport mode. Given the spatial heterogeneity of land use patterns in most cities, large-scale UAM will likely be deployed in specific areas, e.g., inter-transfer traffic between suburbs and city centers. However, large-scale UAM operations connecting multiple origin-destination pairs raise concerns about air traffic safety and efficiency with respect to conflict movements, particularly at large conflict points similar to roadway junctions. In this work, we propose an operational framework that integrates route guidance and collision avoidance to achieve an elegant trade-off between air traffic safety and efficiency. The route guidance mechanism aims to optimize aircraft distribution across both spatial and temporal dimensions by regulating their paths (composed of waypoints). Given the optimized paths, the collision avoidance module aims to generate collision-free aircraft trajectories between waypoints in 3D space. To enable large-scale operations, we develop a fast approximation method to solve the optimal path planning problem and employ the velocity obstacle model for collision avoidance. The proposed route guidance strategy significantly reduces the computational requirements for collision avoidance. As far as we know, this work is one of the first to combine route guidance and collision avoidance for UAM. The results indicate that the framework can enable efficient and flexible UAM operations, such as air traffic assignment, congestion prevention, and dynamic airspace clearance. Compared to the management scheme based on air corridors, the proposed framework has considerable improvements in computational efficiency (433%), average travel speed (70.2%), and trip completion rate (130%). The proposed framework has demonstrated great potential for real-time traffic simulation and management in large-scale UAM systems.

Keywords: Urban air mobility, Multi-agent system, Collision avoidance, Air traffic congestion, Route guidance

1. Introduction

With network capacity approaching saturation, traffic congestion in metropolises becomes a recurrent puzzle. Simply expanding roadway infrastructure is no longer a sustainable solution to meet the increasing demand. Instead, exploring innovative transport modes is more viable to expand the supply of urban mobility. Recently, low-altitude airspace (an underused resource for urban mobility) has gained increased attention for its potential to support point-to-point air travel in congested cities. Advances in machine intelligence, autonomy, and battery technologies will enable electric vertical take-off and landing vehicles (eVTOLs) to become a safe, affordable, and environmentally friendly mode of urban mobility (Holden, 2018; Kasliwal et al., 2019). As a result, urban air mobility (UAM) has emerged with the vision of opening altitude dimensions for urban transport to mitigate roadway traffic congestion. With the

*Corresponding author.

Email addresses: wengcq@mail2.sysu.edu.cn (Canqiang Weng), can-caesar.chen@connect.polyu.hk (Can Chen), tanjj7@mail2.sysu.edu.cn (Jingjun Tan), pantl@pcl.ac.cn (Tianlu Pan), zhrenxin@mail.sysu.edu.cn (Renxin Zhong)

¹The authors contributed equally as the first author.

aid of ride-hailing apps like Lyft or Uber, the viability of large-scale UAM has been evidenced by the test flights of full-size eVTOLs (Dietrich and Wulff, 2020; Garrow et al., 2021). In the coming decade, the UAM market is projected to contribute up to \$700 billion (RMB 5 trillion) to the country’s economy of China (Shen et al., 2023).

As the large-scale deployment of UAM approaches, concerns about air traffic safety and efficiency are increasing. Safety concerns focus on collision avoidance for individual aircraft. Recent studies suggest that new approaches, distinct from the conventional scheme of pre-planned routes and fixed schedules, need to be developed to address potential conflicts among multiple aircraft (Haddad et al., 2021; Safadi et al., 2023a). Efficiency concerns emphasize the prevention of air traffic congestion for UAM systems. Recent studies indicate that UAM systems face congestion issues similar to roadway traffic (Cummings and Mahmassani, 2024a,b). To address safety and efficiency concerns, we need to investigate: (i) *individual traffic behavior of UAM aircraft*; and (ii) *collective traffic behavior of UAM aircraft*.

The microscopic behavior of individual aircraft is typically modeled as point-to-point motion in 2D or 3D space, with the requirement of avoiding collisions with obstacles, such as buildings, and other aircraft. Collision avoidance is a critical issue in UAM systems and, more generally, in multi-agent systems (composed of vehicles). Various algorithms have been reported over the past decade, see e.g., Huang et al. (2019); Yasin et al. (2020) and the literature therein. Some representative works are summarized in Table 1. In general, there are two strategies for collision avoidance: centralized solutions and distributed solutions. In centralized solutions, a hypothetical manager collects all relevant information (e.g., agents’ positions and velocities) and uses it to optimize the decisions for all agents, see e.g., Bahabry et al. (2019); Tang et al. (2021). The manager’s commands are assumed to be followed by all agents, without considering uncertainties, such as the compliance of pilots. In distributed solutions, each agent collects limited information within its detection range and uses it to make decisions, see e.g., Van Den Berg et al. (2011); Long et al. (2017). An agent may be able to perceive the decisions of adjacent agents but cannot directly change their decisions. In this context, the centralized strategy implies global optimal but requires mass computation. While the distributed strategy implies local optimal, it has advantages in terms of computational efficiency.

Table 1: A brief survey of collision avoidance algorithms.

	Strategy	Scenario	Methodology	Objective (<i>minimize</i>)
Jose and Pratihari (2016)	Centralized	2D grid network	A* and GA ^a	Total time spent / fuel consumption
Xue and Do (2019)	Centralized	2D space without obstacle	MILP ^b	Deviation from the reference trajectory
Alrifaae et al. (2014)	Centralized	2D space with obstacle	MPC ^c	Deviation from the reference trajectory
Bahabry et al. (2019); Tang et al. (2021)	Centralized	3D airline network	MILP ^b	Total time spent / total flying cost
Yang and Wei (2020)	Distributed	2D space without obstacle	Game Theory ^d	Total time spent
Quan et al. (2021)	Distributed	3D space with obstacle	APF ^e	Deviation from the reference trajectory
Van Den Berg et al. (2011)	Distributed	2D/3D space with obstacle	VO ^f	Deviation from the reference velocity
Long et al. (2017)	Distributed	2D/3D space without obstacle	DNN ^g	—

- ^a Genetic Algorithm
- ^b Mixed Integer Linear Program
- ^c Model Predictive Control
- ^d Logit level-k model
- ^e Artificial Potential Field
- ^f Velocity Obstacles
- ^g Deep Neural Network

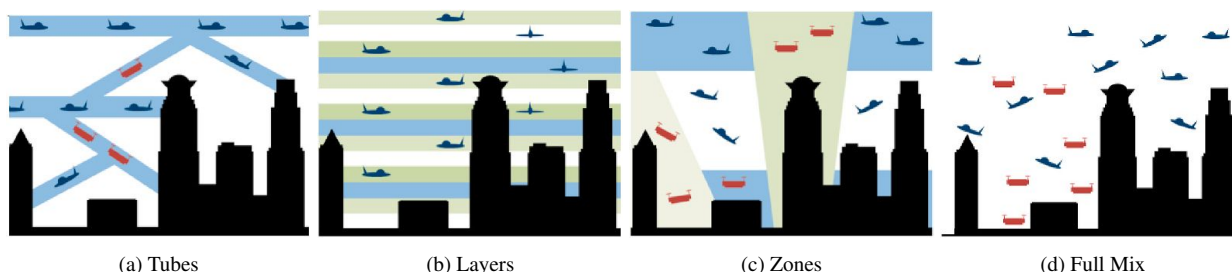


Figure 1: Different airspace structure designs for UAM, ordered by degrees of freedom (Sunil et al., 2015).

In the early deployment of UAM, structured airspace is used to reduce the risk of aircraft collisions. The design

concept of airspace structure is to separate aircraft with different properties (e.g., speed, direction, and level of autonomy) using airspace barriers. A comprehensive review of airspace structure designs is available in the work (Bauranov and Rakas, 2021). To be concise, we summarize some key points. (i) The airspace structures proposed in academia and industry can be roughly categorized into four concepts, i.e., tube, layer, zone, and full mix (see Figure 1) and their integration. For example, the multi-layer sky lanes design (Jang et al., 2017) and the multi-layer air corridors design (Bradford, 2020) integrate the concepts of layers and tubes. (ii) Less structured airspace allows aircraft to fly with more degrees of freedom, leading to higher traffic density. However, high-density aircraft flying freely along self-preferred (often direct) routes would increase the chance of traffic congestion.

Although airspace structures provide a rule-based traffic scheme for UAM in its early stages, further investigation into air traffic management is needed to address future demands. Relevant studies in this area are being led by the US and Europe. NASA proposed the original concept of operations (ConOps) for unmanned aerial vehicle traffic management (UTM), see e.g., Kopardekar et al. (2016). Similarly, the European version of UTM is known as urban space (U-space), see e.g., SESAR Joint Undertaking (2017). A detailed discussion and comparison of the UTM and U-space ConOps can be found in Shrestha et al. (2021). The proposed ConOps is a type of guidelines that explain the functions of system components and how they work together (Shrestha et al., 2021). Under the current UTM architecture, point-to-point operations relying on human operators have limitations on deployment scale. However, both UTM and U-space envision a future of large-scale UAM services with high-level autonomy. In this context, air traffic congestion caused by high-density UAM aircraft attracts more and more attention. Cummings and Mahmassani (2024a) simulated point-to-point UAM operations in 3D space using a decentralized conflict resolution. Their simulations indicate that UAM faces similar congestion issues similar to roadway traffic. In further research, Cummings and Mahmassani (2024b) evaluated air traffic congestion across different airspace structure designs and suggested that advanced routing algorithms may help address these congestion issues. Safadi et al. (2023a) expanded the simulation scale and obtained complete relationships between air traffic flow, density, and speed. The air traffic flow is observed as a concave curve with respect to air traffic density, where the critical density provides a benchmark for identifying air traffic congestion (Cummings and Mahmassani, 2024a). Based on the flow-density relationship, also known as the Macroscopic Fundamental Diagram (MFD), a few approaches have been proposed to manage air traffic congestion (see e.g., Haddad et al., 2021; Safadi et al., 2023b).

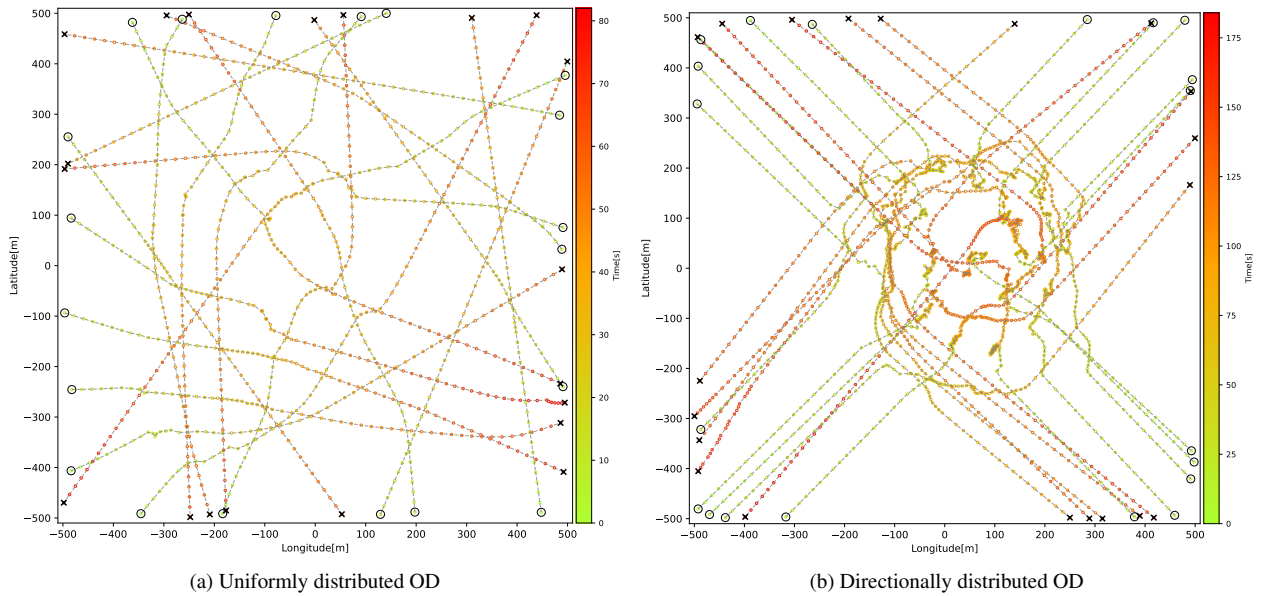


Figure 2: Collision-free aircraft trajectories in 2D space with a deployment scale of 20, where ‘O’ marks the origin and ‘X’ marks the destination. Compared to homogeneous OD in (a), heterogeneous OD in (b) poses higher risks of delay and congestion.

Remarkably, the MFD framework implicitly assumes that traffic congestion is evenly distributed, i.e., the areas with an MFD should be (roughly) homogeneously loaded (Geroliminis and Sun, 2011). To meet this assumption,

most current studies simplify UAM demand by setting the origin-destination (OD) to be uniformly distributed (Haddad et al., 2021; Safadi et al., 2024). However, it is hard to construct a uniformly distributed vertiport network² for UAM in practice, as land use patterns in most cities are spatially heterogeneous (Wu and Zhang, 2021). It is more likely that large-scale UAM will be deployed between specific areas, for example, from the suburbs to city centers. Different settings of OD distribution would lead to significant differences in air traffic operation. As illustrated in Figure 2, potential aircraft conflicts are evenly distributed for uniformly distributed OD, while they are concentrated at the intersection for directionally distributed OD. Similar phenomena of aircraft conflict at intersections are observed in the work (Cummings and Mahmassani, 2024b). Under the same deployment scale, heterogeneous demand, compared to homogeneous demand, leads to higher risks of delay and congestion. As far as we know, investigating air traffic management schemes for spatially heterogeneous demand is practically significant but has not received much attention.

To fill the above research gaps, we propose an operational framework that integrates route guidance and collision avoidance for large-scale UAM. The main contributions of this paper are summarized as follows:

1. To the best of our knowledge, this work is one of the first to integrate route guidance and collision avoidance in the field of UAM. The proposed route guidance strategy optimizes aircraft distribution by regulating their paths (composed of waypoints), while the collision avoidance algorithm generates collision-free aircraft trajectories between given waypoints in 3D space. The route guidance mechanism considerably reduces the computational requirements for collision avoidance. In this way, the framework achieves an elegant trade-off between air traffic safety and efficiency.
2. The proposed framework enables efficient and flexible operations for large-scale UAM, such as air traffic assignment, congestion prevention, and dynamic airspace clearance. By introducing the route guidance mechanism, aircraft are appropriately assigned across both spatial and temporal dimensions, which ensures air traffic homogeneity even for spatially heterogeneous demand. Compared to the management scheme based on air corridors, the proposed framework has considerable improvements in computational efficiency (433%), average travel speed (70.2%), and trip completion rate (130%).

The remainder of this paper is organized as follows: Section 2 introduces the methodology of the proposed framework, including the methods for collision avoidance and route guidance. Section 3 evaluates the performance of the proposed framework through a series of experiments. Section 4 concludes this paper and discusses potential improvements for future work.

2. Large-scale UAM with collision avoidance and route guidance

The workflow of the proposed framework is illustrated in Figure 3. First, settings for the airspace (e.g., region division), aircraft (e.g., safety radius, maximum speed), and UAM demand (e.g., aircraft ODs, departure flow) are input to initialize the environment. Next, necessary information (e.g., aircraft position, velocity) is collected from the environment to assist in decision-making at each time step t_k . The decision-making process consists of two modules: route guidance and collision avoidance. At each time step t_k , the route guidance module updates paths for all aircraft if necessary, as detailed in Section 2.2. Otherwise, the paths³ remain consistent with those from the previous time step t_{k-1} . Here a path for aircraft routing refers to a sequence of waypoints corresponding to the airspace region division. Based on the path decision, the collision avoidance module generates velocity commands to guide aircraft to travel between waypoints, as detailed in Section 2.1. Lastly, the decision-making process is repeated until the mission is complete (i.e., $t_k = t_f$).

2.1. Velocity obstacle model for individual aircraft collision avoidance

In this section, we model the individual traffic behavior of UAM aircraft as point-to-point motion in 3D space and introduce the collision avoidance module of the proposed framework. As summarized in Table 1, various methods are alternatives. Recently, Safadi et al. (2023a) evaluated the Artificial Potential Field (APF) approach for collision-free

²The vertiport network, which is regarded as the OD of air traffic in this paper, is the infrastructure for UAM aircraft to take off and land.

³The initial path of each aircraft is a direct route from the origin to the destination.

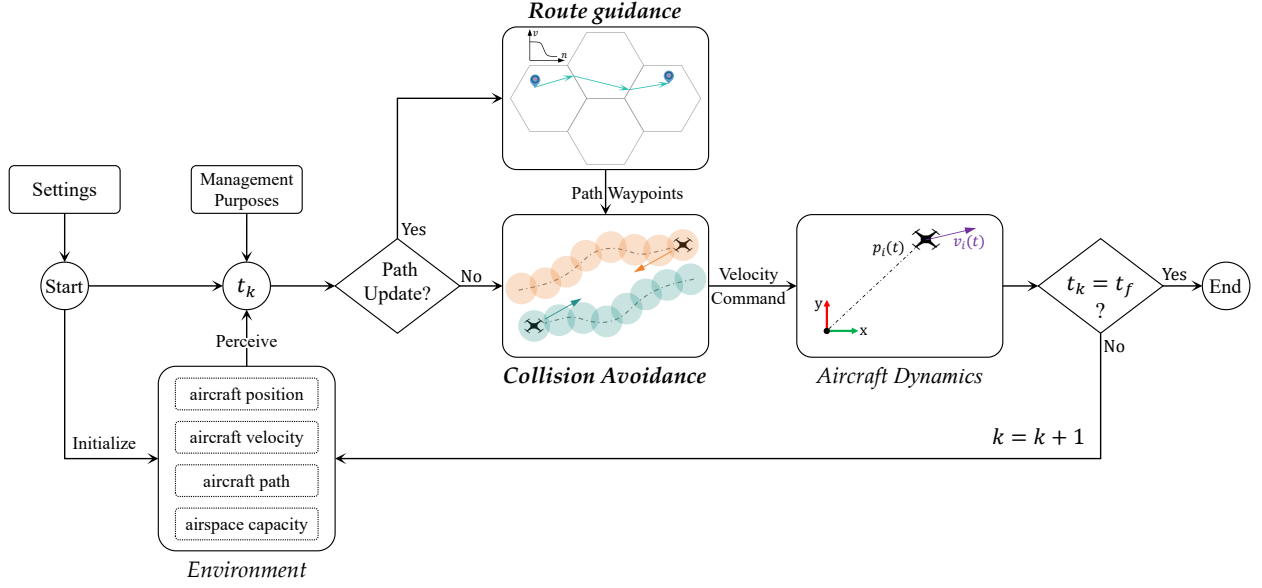


Figure 3: The proposed framework integrates collision avoidance and route guidance for large-scale UAM simulation and management.

flights of UAM. To provide additional insights, this paper employs the Velocity Obstacles (VO) model to achieve collision avoidance for multiple aircraft in both 2D and 3D space. The VO model exhibits good properties in terms of geometric interpretation and computational efficiency, see e.g., [Van Den Berg et al. \(2011\)](#); [Long et al. \(2017\)](#); [Han et al. \(2022\)](#).

We consider aircraft $A_i \in \mathbb{U}_A$, where \mathbb{U}_A is the set of aircraft in the available airspace. Then, the position and velocity of aircraft A_i at time step t_k are denoted by $\mathbf{p}_i(t_k) \in \mathbb{R}^3$ and $\mathbf{v}_i(t_k) \in \mathbb{R}^3$, respectively. In this paper, we suppose that the aircraft dynamics can be expressed by

$$\mathbf{p}_i(t_{k+1}) = \mathbf{p}_i(t_k) + \mathbf{v}_i(t_k)\Delta t \quad (1a)$$

$$\mathbf{v}_i(t_k) = \mathbf{v}_i^c(t_k) \quad (1b)$$

where $\Delta t = t_{k+1} - t_k > 0$ is the simulation period and $\mathbf{v}_i^c(t_k) \in \mathbb{R}^3$ is the velocity command. Given a saturation function defined as follows

$$\text{sat}(\mathbf{v}, v^{max}) = \begin{cases} \mathbf{v} & , \quad \|\mathbf{v}\| \leq v^{max} \\ v^{max} \frac{\mathbf{v}}{\|\mathbf{v}\|} & , \quad \|\mathbf{v}\| > v^{max} \end{cases} \quad (2)$$

the velocity of aircraft A_i should be constrained by its speed limit, i.e., $\mathbf{v}_i = \text{sat}(\mathbf{v}_i, v_i^{max})$ and $\mathbf{v}_i^c = \text{sat}(\mathbf{v}_i^c, v_i^{max})$, where v_i^{max} is the maximum speed of aircraft A_i . Remarkably, the dynamics (1) implicitly assume that aircraft have sufficient mobility to adjust the current velocity $\mathbf{v}_i(t_k)$ to the commanded velocity $\mathbf{v}_i^c(t_k)$ within Δt time. The assumption implies that the maximum acceleration of aircraft A_i should satisfy $a_i^{max} \geq 2v_i^{max}/\Delta t$.

As designed, the velocity command $\mathbf{v}_i^c(t_k)$ needs to (i) guide aircraft A_i to approach its destination, and (ii) avoid collision with other aircraft. In the literature, objective (i) is widely formulated as minimizing the gap between the velocity command and the preferred velocity, i.e., $\min \|\mathbf{v}_i^c - \mathbf{v}_i^p\|$, where the preferred velocity $\mathbf{v}_i^p \in \mathbb{R}^3$ is typically selected as the maximum velocity from the current position to the destination. For objective (ii), we introduce $ORCA_{A_i}^\tau$ as the set of permitted velocities that enables aircraft A_i to avoid collisions with other aircraft, referring to [Van Den Berg et al. \(2011\)](#); [Han et al. \(2022\)](#). Then the overall objective is to select a velocity from the permitted set to be as close as possible to the preferred velocity, i.e.,

$$\mathbf{v}_i^c(t_k) = \arg \min_{\mathbf{v} \in ORCA_{A_i}^\tau} \|\mathbf{v} - \mathbf{v}_i^p(t_k)\| \quad (3)$$

The permitted velocities of aircraft A_i are influenced by other aircraft within the detection range, which implies

$$ORCA_{A_i}^\tau = \bigcap_{A_j \in \mathbb{N}_i} ORCA_{A_i|A_j}^\tau \quad (4)$$

where \mathbb{N}_i is the set of aircraft within the detection range of aircraft A_i , and $ORCA_{A_i|A_j}^\tau$ is the set of permitted velocities for aircraft A_i induced by aircraft A_j . Remarkably, the collision avoidance mechanism is only triggered for aircraft when detecting potential conflicts (i.e., $\mathbb{N}_i \neq \emptyset$). In other words, collision avoidance can be significantly simplified if aircraft are appropriately guided, for example, by path planning.

Since the objective function is quadratic with a single minimum, problem (3) can be easily solved if the permitted velocity constraints $\mathbf{v} \in ORCA_{A_i}^\tau$ are provided. Based on the VO model, Van Den Berg et al. (2011) derived the sufficient conditions for collision-free motion of multiple agents. Their work geometrically parses the permitted velocity constraints and reformulates them as linear constraints. To acknowledge their contribution, we recommend that readers refer to the original work for details. Nevertheless, we provide a brief version of the derivation of the permitted velocity constraints here.

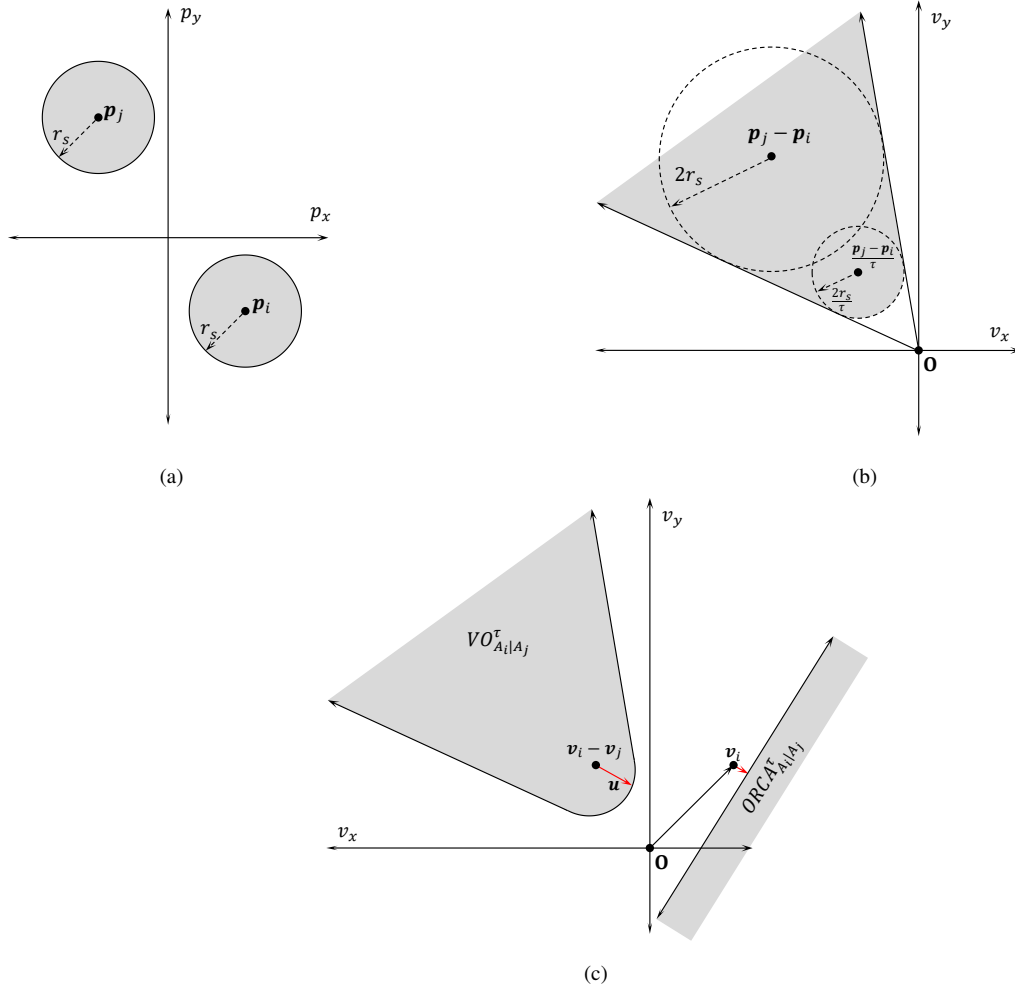


Figure 4: (a) The collision-free configuration of aircraft A_i and A_j with non-overlapping safety ranges; (b) The velocity obstacle $VO_{A_i|A_j}^\tau$ is a truncated cone (in velocity space) with its apex at the origin and its legs tangent to the disc of radius $2r_s$ centered at $\mathbf{p}_j - \mathbf{p}_i$; (c) The set $ORCA_{A_i|A_j}^\tau$ of permitted velocities for aircraft A_i induced by aircraft A_j is a half-plane pointing in the direction of \mathbf{u} starting at the point $\mathbf{v}_i + \frac{1}{2}\mathbf{u}$, where \mathbf{u} is the vector from $\mathbf{v}_i - \mathbf{v}_j$ to the closest point on the boundary of $VO_{A_i|A_j}^\tau$.

We derive the permitted velocity constraints as follows, beginning with 2D space for simplicity. Let $D(\mathbf{p}, r)$ denote an open disc of radius r centered at position \mathbf{p} , i.e.,

$$D(\mathbf{p}, r) = \{\mathbf{q} \mid \|\mathbf{q} - \mathbf{p}\| < r\} \quad (5)$$

As illustrated in Figure 4a, two aircraft A_i and A_j are considered collision-free if their safety ranges do not overlap, which implies $D(\mathbf{p}_i, r_s) \cap D(\mathbf{p}_j, r_s) = \emptyset$. Then we introduce the velocity obstacle ⁴ $VO_{A_i|A_j}^\tau$ as the set of all relative velocities of aircraft A_i with respect to aircraft A_j that will result in a collision at some moment before time τ . Mathematically, $VO_{A_i|A_j}^\tau$ is defined as follows

$$VO_{A_i|A_j}^\tau = \{\mathbf{v} \mid \exists t \in [0, \tau] : \mathbf{v}t \in D(\mathbf{p}_j - \mathbf{p}_i, 2r_s)\} \quad (6)$$

Here, the auxiliary variable $t \in [0, \tau]$, not to be confused with the discrete decision time t_k , is used to define the continuous set $VO_{A_i|A_j}^\tau$. The geometric interpretation of the velocity obstacle $VO_{A_i|A_j}^\tau$ is a truncated cone (in velocity space), as shown in Figure 4b. Given aircraft velocities \mathbf{v}_i and \mathbf{v}_j , the relative velocity of aircraft A_i with respect to aircraft A_j is $\mathbf{v}_i - \mathbf{v}_j$. The definition of the velocity obstacle implies that if $\mathbf{v}_i - \mathbf{v}_j \in VO_{A_i|A_j}^\tau$, then aircraft A_i and A_j will collide at some moment before time τ if their velocities do not change. Conversely, if $\mathbf{v}_i - \mathbf{v}_j \notin VO_{A_i|A_j}^\tau$, aircraft A_i and A_j are guaranteed to be collision-free for at least time τ . For the collision case, let \mathbf{u} be the vector from $\mathbf{v}_i - \mathbf{v}_j$ to the closest point on the boundary of the velocity obstacle $VO_{A_i|A_j}^\tau$ as follows

$$\mathbf{u} = \left(\arg \min_{\mathbf{v} \in \partial VO_{A_i|A_j}^\tau} \|\mathbf{v} - (\mathbf{v}_i - \mathbf{v}_j)\| \right) - (\mathbf{v}_i - \mathbf{v}_j) \quad (7)$$

The geometric interpretation of vector \mathbf{u} is the minimum variation in relative velocity $\mathbf{v}_i - \mathbf{v}_j$ to move out of the velocity obstacle, as illustrated in Figure 4c. To fairly share the responsibility for collision avoidance, we assume that aircraft A_i and A_j each take half of the responsibility for the minimum velocity variation \mathbf{u} . In this way, aircraft A_i should adapt its velocity by at least $\frac{1}{2}\mathbf{u}$, which implies that the permitted velocities of aircraft A_i should lie in the half-plane pointing in the direction of \mathbf{u} starting at the point $\mathbf{v}_i + \frac{1}{2}\mathbf{u}$. More formally, we have

$$ORCA_{A_i|A_j}^\tau = \{\mathbf{v} \mid (\mathbf{v} - (\mathbf{v}_i + \frac{1}{2}\mathbf{u})) \cdot \mathbf{u} \geq 0\} \quad (8)$$

The geometric interpretation of $ORCA_{A_i|A_j}^\tau$ is a half-plane (in velocity space), as shown in Figure 4c. So far, the permitted velocity constraints of aircraft A_i induced by aircraft A_j are derived and reformulated as linear constraints. More generally, the derivation of the permitted velocity constraints in 3D space is quite similar to the case in 2D space and is not repeated.

2.2. Region-based route guidance for collective aircraft management

In this section, we devise a region-based optimal route guidance strategy for regulating the collective aircraft behavior to alleviate traffic congestion in the airspace. With the VO model to regulate the individual behavior of UAM aircraft, one can ensure a collision-free UAM traffic but may not be able to protect the UAM airspace from over-saturation. As illustrated in Figure 2, simply relying on collision avoidance for motion decisions may lead multiple aircraft to simultaneously enter the same airspace (region), significantly increasing the risk of traffic congestion and even gridlock. Severe local congestion, in turn, significantly increases the chances of triggering the collision avoidance mechanism, which requires considerable computational resources and may influence the real-time feasibility of large-scale UAM simulation. Similar results have been reported in the literature, along with suggestions for advanced routing algorithms, see e.g., Safadi et al. (2023a); Cummings and Mahmassani (2024b). On the other hand, previous studies on urban road network traffic management showed that an appropriate regional route guidance strategy not only alleviates the traffic congestion for certain regions (e.g., the CBD area) but also improves the overall network

⁴ $VO_{A_i|A_j}^\tau$ is read as the velocity obstacle for aircraft A_i induced by aircraft A_j for time window τ .

performance (Li and Ramezani, 2022; Chen et al., 2024). Operations of UAM should be more flexible than those of urban road networks because the vertical space can be used for both collision avoidance and route planning. This enables us to design a computation-efficient route guidance mechanism to optimize aircraft distribution across both spatial and temporal dimensions by regulating their paths. We will show in later sections the proposed region-based route guidance strategy can retain air traffic homogeneity even in cases of spatially heterogeneous demand. Moreover, the proposed route guidance algorithm can significantly reduce the search space when approximating the optimal route guidance strategy.

2.2.1. Optimal path planning based on 4D trajectories prediction

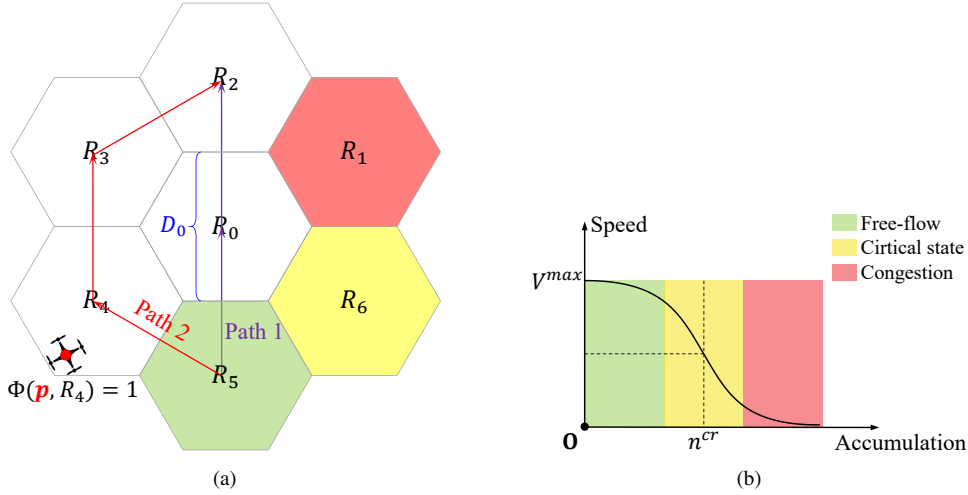


Figure 5: (a) Schematic of airspace region division (top view); (b) The relationship between aircraft travel speed and accumulation within an airspace region during 4D trajectory prediction.

We consider the available airspace without static obstacles and divide the airspace into several non-overlapping regions, as illustrated in Figure 5a. Inspired by cellular communication, we employ hexagonal region division in this work. Let $R_l \in \mathbb{U}_R$ represent an airspace region, where \mathbb{U}_R is the set of regions within the available airspace. Accordingly, we denote a path $P_i \in \mathbb{P}_i$ for aircraft A_i to travel from its current position $\mathbf{p}_i(t_k)$ to the destination \mathbf{d}_i , where \mathbb{P}_i is the set of candidate paths for aircraft A_i . The candidate paths between two regions can be pre-defined as a few simple short paths (e.g., by Dijkstra’s algorithm).

First we investigate the path planning for N aircraft $A_i \in \mathbb{U}_A, i = 1, \dots, N$. Path planning requires consideration of both spatial and temporal dimensions to prevent multiple aircraft from entering the same airspace region simultaneously. Inspired by model predictive control (MPC), we predict 4D aircraft trajectories (spatio-temporal aircraft trajectories in 3D space) to evaluate the path decision at the current time step t_k . Given a path P_i , we use the dynamics (1) to predict the future trajectory for aircraft A_i . To avoid confusion, the time variable t_k is replaced by t_p in predicting 4D aircraft trajectories. For simplicity, the velocity command $\mathbf{v}_i^c(t_p)$ is set to be the preferred velocity directed from the aircraft’s current position $\mathbf{p}_i(t_p)$ to the next waypoint along path P_i . Note that we do not consider collision avoidance when predicting aircraft 4D trajectories. That is, $\mathbf{v}_i^c(t_p)$ is merely used for trajectory prediction and will not affect the velocity command output by the VO model if the collision avoidance mechanism is triggered. On the one hand, predicting collision-free aircraft trajectories requires additional computation but has little improvement in evaluating path decisions. On the other hand, appropriate path decisions would effectively alleviate local traffic congestion, and thus reduce the chance of triggering the collision avoidance mechanism.

To capture the influence of regional traffic congestion, we assume that the aircraft travel speed would decrease as aircraft accumulation increases within an airspace region. The aircraft accumulation within airspace region R_l can be calculated as follows

$$n_l(t_p) = \sum_{A_i \in \mathbb{U}_A} \Phi(\mathbf{p}_i(t_p), R_l) \quad (9)$$

where $\Phi(\mathbf{p}_i, R_l) = \begin{cases} 1, & \text{if } \mathbf{p}_i \in R_l \\ 0, & \text{otherwise} \end{cases}$ is an indicator function to declare whether aircraft A_i (located at \mathbf{p}_i) is within airspace region R_l . Inspired by Wang et al. (2011), we define the relationship between aircraft accumulation and travel speed as follows

$$V_{R_l}(t_p) = \frac{\exp(n_l^{cr} - n_l(t_p))}{1 + \exp(n_l^{cr} - n_l(t_p))} V_{R_l}^{max} \quad (10)$$

where parameters n_l^{cr} and $V_{R_l}^{max}$ represent the critical accumulation and maximum travel speed of airspace region R_l , respectively. This speed-accumulation relationship is illustrated in Figure 5b, depicting three traffic states: free flow, critical, and congestion. Then we regard equation (10) as a rough estimation of the speed of aircraft A_i with current position $\mathbf{p}_i \in R_l$ at time step t_p . Hence, we have $\forall A_i \in \mathbb{U}_A, \|\mathbf{v}_i^c(t_p)\| = V_{R_l}(t_p)$, if $\Phi(\mathbf{p}_i(t_p), R_l) = 1$. In this manner, the 4D aircraft trajectories and regional traffic states interact with each other. By iterating between (9) and (10), we alternately update the aircraft's velocity commands $\mathbf{v}_i^c(t_p)$ and regional traffic accumulation $n_l(t_p)$ to obtain 4D aircraft trajectories.

Using the predicted aircraft trajectories, we evaluate the corresponding path decision based on the total time spent by all aircraft. At decision time step t_k , the predicted time spent for aircraft A_i is calculated by

$$PTS_i = t_{e,i} - t_k \quad (11)$$

where $t_{e,i}$, satisfying $\mathbf{p}_i(t_{e,i}) = \mathbf{d}_i$, is the time at which aircraft A_i reaches its destination. Thus, the path planning for N aircraft at time step t_k is designed to select optimal paths from the candidate paths to minimize the total time spent by all aircraft, i.e.,

$$\min_{P_1, P_2, \dots, P_N} TTS = \sum_{A_i \in \mathbb{U}_A} PTS_i \quad (12)$$

Problem (12) is a Combinatorial Optimization problem, with the search space containing every combination of the N aircraft's paths. Thus, the size of the search space is M^N , where N is the number of aircraft and M is the number of candidate paths for each aircraft. For each path combination within the search space, we need to predict the corresponding 4D aircraft trajectories to calculate the total time spent. In this context, searching for the optimal solution to problem (12) is computationally intensive, making exhaustive search infeasible for large-scale problems. Therefore in Section 2.2.2, we develop a fast approximation method (FAM) with high computational efficiency to provide an approximate optimal solution to problem (12). The proposed FAM reduces the search space from M^N to MN , with the solution being very close to the optimal one (as will be shown by numerical results in Section 3).

2.2.2. Fast approximation method to approach the optimal route guidance strategy

Now we devise a fast approximation method (FAM) to solve problem (12). Note that using the 4D aircraft trajectories to calculate the total time spent is the most basic operation in solving problem (12). Thus, we estimate the total time spent in a simplified manner to enhance computational efficiency. We consider N aircraft with each aircraft A_i given path P_i , $i = 1, \dots, N$. Accordingly, the 4D aircraft trajectories are determined by the path combination $[P_1, P_2, \dots, P_N]^T$. Since traffic congestion in specific regions would significantly increase total time spent, the (roughly) uniform distribution of aircraft trajectories is more likely to be the optimal solution. We consider the path combination $[P_1, P_2, \dots, P_N]^T$ as an accepted solution, resulting in a (roughly) uniform distribution of aircraft trajectories. In this context, the travel speed of aircraft can be regarded as roughly equivalent in each region. Thus, we can align the path combination $[P_1, P_2, \dots, P_N]^T$ by regions as follows

$$\begin{bmatrix} P_1 \\ P_2 \\ \vdots \\ P_i \\ \vdots \\ P_N \end{bmatrix} = \begin{bmatrix} R_{1,1}, & R_{1,2}, & \dots \\ R_{2,1}, & R_{2,2}, & \dots \\ \vdots & \vdots & \ddots \\ R_{i,1}, & R_{i,2}, & \dots \\ \vdots & \vdots & \ddots \\ R_{N,1}, & R_{N,2}, & \dots \end{bmatrix}_{N \times L} \quad (13)$$

where $R_{i,j}$ is the j -th region that path P_i traverses and L is the length of paths. Here, the paths are padded (e.g., with null values) to ensure their lengths are equivalent.

The first step of the proposed FAM is to estimate the total time spent based on collective states (13), rather than individual trajectories (11). To be specific, we introduce $S_1 = [R_{1,1}, R_{2,1}, \dots, R_{i,1}, \dots, R_{N,1}]^T$ to describe the state of aircraft traveling in the first regions of their respective paths. Then the aircraft accumulation of region R_l corresponding to state S_1 can be calculated as follows

$$n_l(S_1) = \text{COUNT}(S_1, R_l), \forall R_l \in \mathbb{U}_R \quad (14)$$

where $\text{COUNT}(S_1, R_l)$ is to count the number of R_l occurs in S_1 . Accordingly, the aircraft travel speed within region R_l is estimated as follows

$$V_{R_l}(S_1) = \frac{\exp(n_l^{cr} - n_l(S_1))}{1 + \exp(n_l^{cr} - n_l(S_1))} V_{R_l}^{max}, \forall R_l \in \mathbb{U}_R \quad (15)$$

Thus we can calculate the travel time spent corresponding to state S_1 as follows

$$T(S_1) = \sum_{R_l \in \mathbb{U}_R} \frac{D_l}{V_{R_l}(S_1)} \cdot n_l(S_1) \quad (16)$$

where D_l is the average travel distance for aircraft in airspace region R_l . By summing up the travel time spent corresponding to each discrete state S_k , we can estimate the total time spent as

$$TTS = \sum_{k=1}^L T(S_k) \quad (17)$$

The estimation method described above involves only simple matrix operations, which ensures high computational efficiency.

Now we propose a multiple-stage decision method to solve the route guidance problem (12). Recall that the original combinatorial optimization problem (12) requires extensive computational effort in solving the single-stage optimization problem. To be specific, using a brute-force solution algorithm to solve (12) leads to M^N search times. To reduce the search space, we reformulate problem (12) into a multiple-stage optimization problem. First, we sort the N aircraft by travel distance (i.e., the distance between origin and destination), from smallest to largest. Thus, we obtain the ordered aircraft set as $\{A_1, \dots, A_N\}$ and for each aircraft A_i the candidate path set \mathbb{P}_i . In this first stage, the total time spent is computed using (17), where only aircraft A_1 is considered. Accordingly, we find the optimal path $P_1^* \in \mathbb{P}_1$ that minimizes the total time spent during the first stage by solving

$$P_1^* = \arg \min_{P_1 \in \mathbb{P}_1} PTS_1 \quad (18)$$

Then we update the path combination in (13) with $P_1 = P_1^*$. From the second to the N -th stage, we perform the following procedures: For the i -th stage ($i = 2, \dots, N$), (i) update the path combination with $P_{i-1} = P_{i-1}^*$, and (ii) minimize the total time spent of aircraft $\{A_1, \dots, A_i\}$ with the output of the previous stages' optimization fixed, i.e., find the i -th optimal path $P_i^* \in \mathbb{P}_i$ by solving

$$P_i^* = \arg \min_{P_i \in \mathbb{P}_i} \sum_{k=1}^i PTS_k \quad (19)$$

subject to $P_k = P_k^*, k = 1, \dots, i-1$

The proposed FAM approach for UAM route guidance is summarized in [Algorithm 1](#). Compared with the exhaustive search algorithm, the scale of search space is reduced from M^N to MN in each stage of finding the optimal path for aircraft A_i . The approximate solution is demonstrated to be very close to the optimal solution, as will be evidenced in the next section.

Algorithm 1: Fast Approximation Method for UAM Route Guidance

input :
Current aircraft positions $\mathbf{p}_i(t_k), i = 1, 2, \dots, N$;
Aircraft destinations $\mathbf{d}_i, i = 1, 2, \dots, N$;
Candidate path set $\mathbb{P}_i, i = 1, 2, \dots, N$

output:
Approximate optimal path combination $[P_1^*, P_2^*, \dots, P_N^*]^T$ for N aircraft

- 1 Sort the N aircraft by the distance from the current position $\mathbf{p}_i(t_k)$ to the destination \mathbf{d}_i (from smallest to largest) and obtain the ordered aircraft set $\{A_1, A_2, \dots, A_N\}$
- 2 Initialize the approximate optimal solution $\mathbf{P}^* \leftarrow []^T$
- 3 **for** $P_1 \in \mathbb{P}_1$ **do**
- 4 | Estimate the total time spent using (17) for aircraft A_1
- 5 **end**
- 6 Solve (18) to find the optimal path P_1^* with minimal total time spent for aircraft A_1 , $\mathbf{P}^* \leftarrow [P_1^*]^T$
- 7 **for** $i \leftarrow 2$ to N **do**
- 8 | Fix the paths of previous $i - 1$ aircraft using the optimal solution $[P_1^*, P_2^*, \dots, P_{i-1}^*]^T$
- 9 | **for** $P_i \in \mathbb{P}_i$ **do**
- 10 | | Estimate the total time spent using (17) for i aircraft A_1, A_2, \dots, A_i
- 11 | **end**
- 12 | Solve (19) to find the optimal path P_i^* with minimal total time spent for aircraft A_i
- 13 | Add the optimal path of aircraft A_i into the optimal solution, i.e., $\mathbf{P}^* \leftarrow [P_1^*, P_2^*, \dots, P_i^*]^T$
- 14 **end**

3. Simulation of large-scale air traffic flow

In this section, we present case studies to evaluate the performance of the proposed framework. We compare the proposed management scheme with the one based on air corridors. Both 2D and 3D space scenarios are investigated for a comprehensive comparison. Qualitative and quantitative analysis of 2D and 3D examples are provided. The compared performance indices include computational efficiency, average travel speed, and trip completion rate. Apart from the performance comparison with the corridor-based management scheme, we present an example to demonstrate our proposed framework's flexibility in UAM operations.

3.1. Simulation settings

As discussed in Section 2, necessary simulation settings include: airspace settings, aircraft settings, and demand settings. We follow the airspace region division in Figure 5a, where the side length of each hexagonal region is set to be $250m$. Here, airspace regions can be considered as a 2D network (i.e., aircraft traveling in the X-Y plane) or a 3D network (i.e., aircraft traveling in the X-Y-Z space). The altitude of airspace regions is set to be $z = 500m$ in 2D examples, while it is set to be $z \in [450, 550]m$ or $z \in [400, 600]m$ in 3D examples. Note that aircraft are free to fly in any direction but must stay inside the network. In this study, all aircraft follow the same settings as follows: the detection radius $r_d = 200m$, safety radius $r_s = 50m$, maximum speed $v^{max} = 20m/s$. And the simulation period is set to be $\Delta t = 1s$. The proposed operational framework is implemented in Python 3.7, on a 64-bit Windows PC with 2.9-GHz Intel Core i7 processor and 36-GB RAM.

3.2. Simulation results

To evaluate the performance of the proposed framework, we first design a baseline for comparison. The baseline simulates the air traffic management scheme based on air corridors (Jang et al., 2017; Kopardekar et al., 2016). As suggested by the FAA, air corridors will connect vertiport networks to support point-to-point operations in the initial phases of UAM. To adapt to large-scale UAM, we allow intersections between air corridors in this study. We design three types of scenarios, as illustrated in Figure 6, with each scenario tested in both 2D space and 3D space. Therefore, there are 9 examples for baseline testing, while Figure 6 only shows 3 examples to save paper length. In each example,

the origins and destinations of all aircraft are randomly generated from two ends of a corridor. Additionally, aircraft are considered free to fly between origins and destinations without collisions, using the method described in Section 2.1. Based on the results of the small-scale test (see Figure 2), it is predicted to occur considerable air traffic congestion at the intersection in large-scale tests. Therefore, we relax the physical constraints of air corridors on aircraft for safety. Specifically, aircraft are permitted to fly outside the air corridors (in terms of longitude and latitude) when necessary, for example, to avoid local deadlocks. Nevertheless, aircraft will travel inside the corridors most of the time, as their origins and destinations are located in corridors. Note that a 3D airspace network would support higher UAM demand compared to a 2D airspace network, as evidenced by Safadi et al. (2023a). Hence, we design three different patterns of aircraft inflow for examples in both 2D and 3D space, as illustrated in Figure 7.

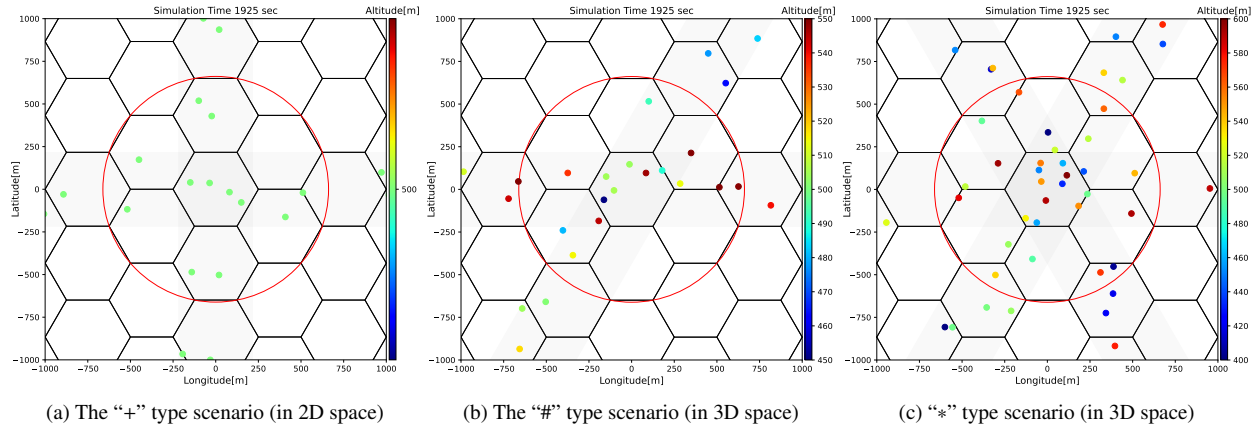


Figure 6: Different testing scenarios of (a) two orthogonal air corridors intersecting; and (b) two oblique air corridors intersecting; and (c) three air corridors intersecting; where air corridors are marked by gray shadows, and aircraft are marked by scatters with their colors indicating altitude.

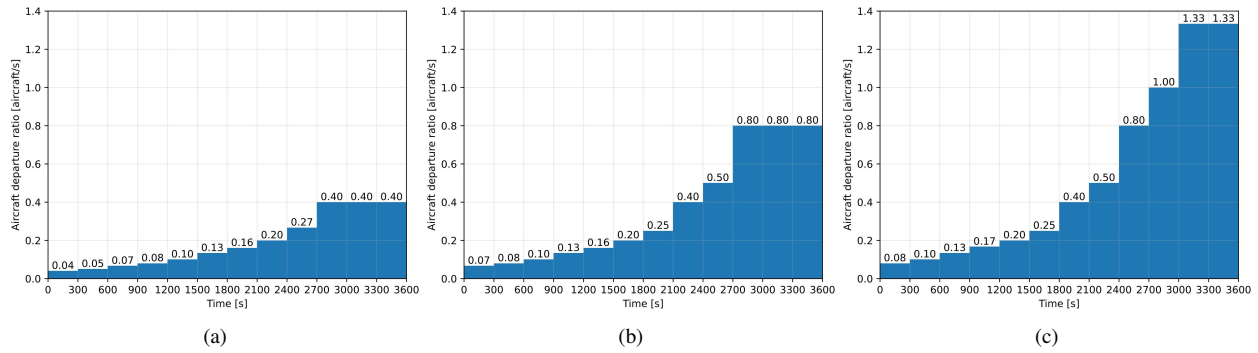


Figure 7: Different aircraft inflow patterns for (a) 2D examples with $z = 500m$; (b) 3D examples with $z \in [450, 550]m$; (c) 3D examples with $z \in [400, 600]m$.

Firstly, simulations in 2D space are conducted. We aggregate the average aircraft accumulation within each airspace region (over a period of 300s) to indicate the level of traffic congestion, represented by a heat map. The results of the baseline in “+” type, “#” type, and “*” type scenarios are illustrated in Figure 8a, Figure 8c, and Figure 8e, respectively. Across different scenarios, the results of air traffic evolution exhibit a similar pattern. With demand loading, more and more aircraft enter the intersection of air corridors, which increases the risk of air traffic congestion. Unfortunately, traffic congestion is likely to escalate once a few aircraft become stuck in a local deadlock at the intersection. Regardless of how the corridors intersect, traffic congestion would originate from the intersection and eventually expand throughout the entire network. Remarkably, similar phenomena have been observed in the practice of roadway traffic over the past decades (Geroliminis and Sun, 2011).

Under the same configuration as the baseline, we conduct simulations to evaluate the performance of the proposed framework. As designed, the route guidance mechanism should enable aircraft to take various paths rather than just the direct route from their origins to destinations. Additionally, the objective of minimizing total travel time spent should lead to an appropriate assignment of aircraft across both spatial and temporal dimensions. The results of the proposed framework meet the above expectations, as illustrated in [Figure 8b](#), [Figure 8d](#), and [Figure 8f](#). Compared to the baseline, aircraft are distributed across more airspace regions, with accumulations in these regions being roughly the same. More importantly, aircraft accumulations in the regions at the intersection are significantly reduced, which successfully prevents air traffic congestion. Regardless of the spatial distribution of aircraft OD (in different scenarios), the proposed framework can effectively ensure air traffic homogeneity.

Secondly, we conduct simulations in 3D space. The qualitative results of the 3D examples are quite similar to those of the 2D examples and are therefore not repeated. To provide quantitative insights, we measure the traffic outflow and accumulation at the intersection, with the measurement range marked by a red circle in [Figure 6](#). The results of outflow-accumulation relationships are illustrated in [Figure 9](#)-[Figure 11](#), including 9 tests in both 2D and 3D spaces, and across different scenarios. In all results of the baseline, the traffic outflow is observed to initially rise and then decrease once aircraft accumulation exceeds a critical value. In the literature, this outflow-accumulation relationship is also called the MFD. Note that the MFDs for the baseline are complete including both ascending and descending phases, which are consistent with the results of [Safadi et al. \(2023a\)](#). The ascending phase is considered to correspond to the free-flow state, while the descending phase corresponds to traffic congestion. In this context, we can conclude that air traffic at the intersection will eventually become congested in all baseline examples (not just the 2D examples in [Figure 8](#)). Conversely, the MFDs for the proposed framework are observed to contain only the ascending phase. In other words, air traffic congestion is effectively prevented in all examples of the proposed framework.

It is also observed that there are considerable disparities in the critical point (marked by “▲” in [Figure 9](#)-[Figure 12](#)) between the 2D and 3D examples. Following [Safadi et al. \(2023a\)](#), we estimate the MFDs with a fitting curve

$$\tilde{G}(N) = \alpha N \exp\left(-\frac{1}{\beta} \left(\frac{N}{N^{cr}}\right)^\beta\right)$$

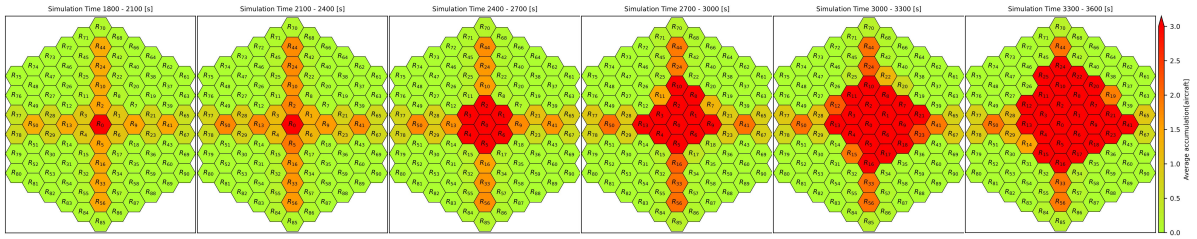
where α , β , and N^{cr} are parameters to be estimated. The critical point of the fitting curve is given by $(N^{cr}, \alpha N^{cr} e^{-\frac{1}{\beta}})$. Under the same settings in 2D space (or 3D space), the critical points across different scenarios show no significant differences. It turns out that the critical point primarily depends on the altitude range of the airspace ⁵. Hence, we aggregate the results from different scenarios and represent them as flow-density relationships to eliminate the impact of the measurement range. The results are illustrated in [Figure 12](#). The aggregated results are more suitable for estimation since the variance is reduced by the increased samples. [Table 2](#) summarizes the estimated metrics of jam density \tilde{K}_{jam} , critical density \tilde{K}_{cr} , and critical flow $\tilde{Q}(\tilde{K}_{cr})$ in 2D space and 3D space. In the literature, these three metrics are regarded as benchmarks for network capacity. As expected, the metrics of network capacity increase with respect to the altitude range of the airspace. Interestingly, the increase is nearly linear. A possible explanation ⁶ is that the airspace for $z \in [400, 600]m$ can be viewed as a stack of two airspace layers for $z \in [450, 550]m$. In this context, the metrics of the $z \in [400, 600]m$ network should double with respect to the $z \in [450, 550]m$ network. Remarkably, the baseline in this study is used not only for comparison but also to provide parameters for the route guidance module, i.e., the critical accumulation n_i^{cr} in equation (10).

Table 2: Capacity estimation for 2D airspace and 3D airspace.

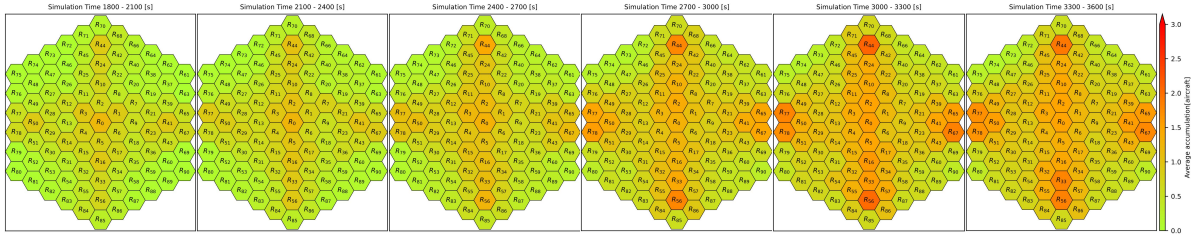
	\tilde{K}_{jam} [aircraft/km ²]	\tilde{K}_{cr} [aircraft/km ²]	$\tilde{Q}(\tilde{K}_{cr})$ [aircraft/s/km ²]
2D results for $z = 500m$	75	13.67	0.10
3D results for $z \in [450, 550]m$	200	27.66 (102% ↑)	0.18 (80% ↑)
3D results for $z \in [400, 600]m$	300	40.75 (198% ↑)	0.28 (180% ↑)

⁵More specifically, the critical point primarily depends on the volume of the airspace.

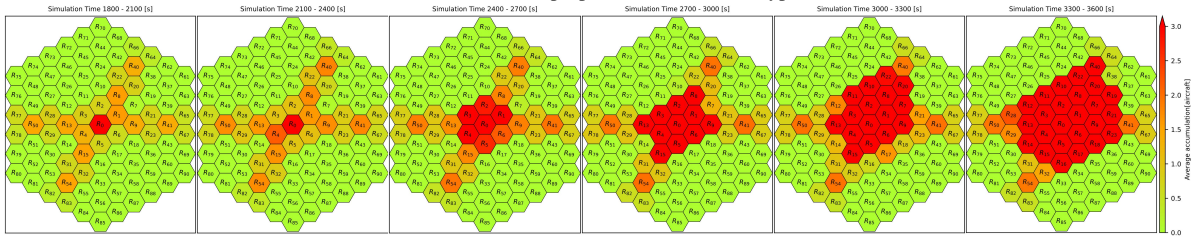
⁶Considering the safety radius of aircraft, the 3D airspace for $z \in [450, 550]m$ can be viewed as a stack of two airspace layers for $z = 500m$.



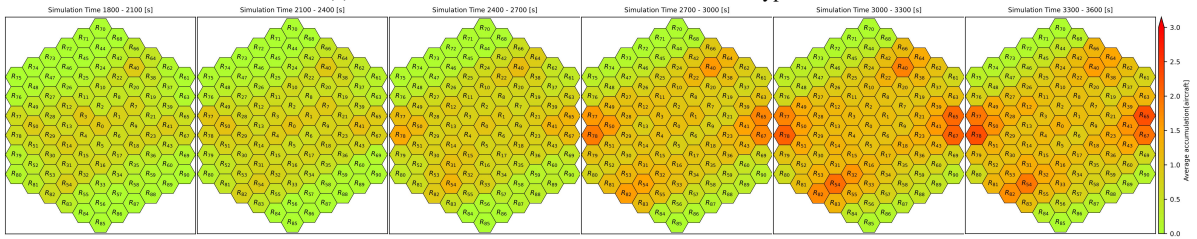
(a) Traffic evolution of the baseline method in “+” type scenario.



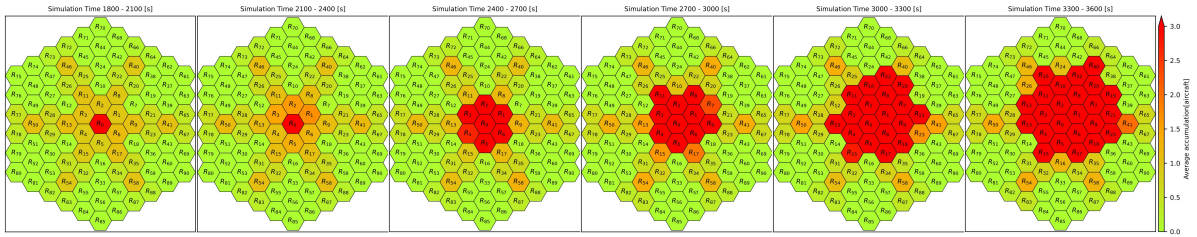
(b) Traffic evolution of the proposed method in “+” type scenario.



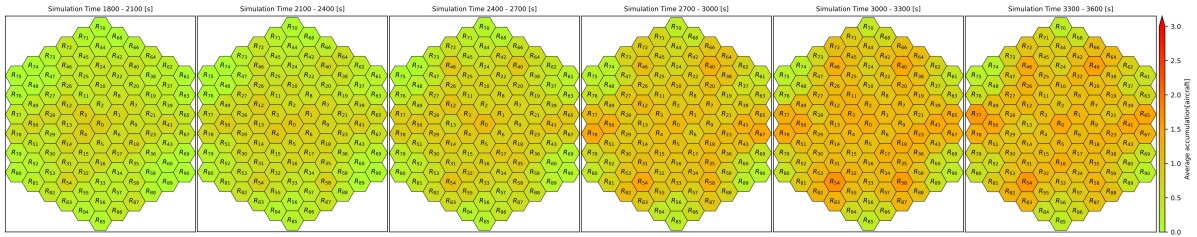
(c) Traffic evolution of the baseline method in “#” type scenario.



(d) Traffic evolution of the proposed method in “#” type scenario.

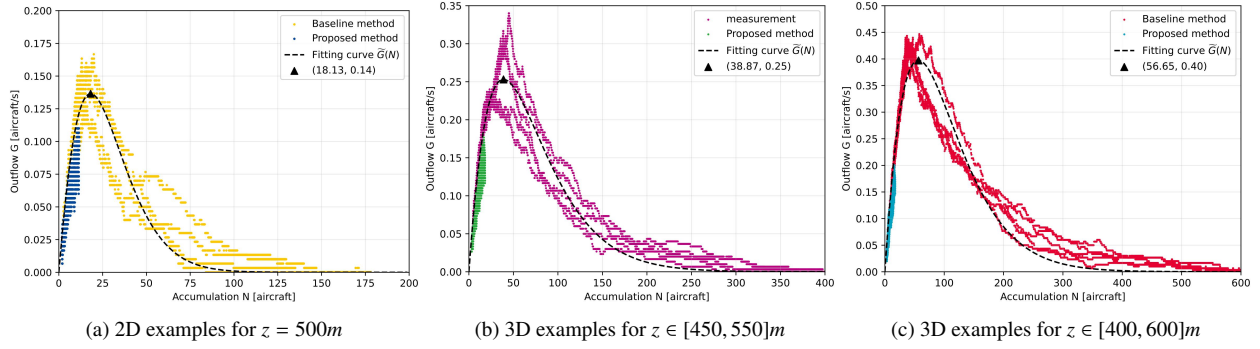


(e) Traffic evolution of the baseline method in “*’” type scenario.



(f) Traffic evolution of the proposed method in “*’” type scenario.

Figure 8: Performance comparison of air traffic evolution in 2D space.

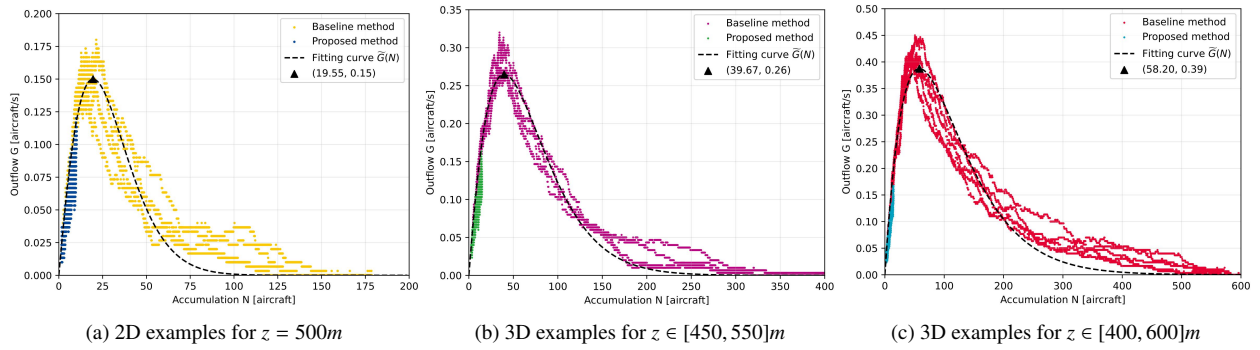


(a) 2D examples for $z = 500m$

(b) 3D examples for $z \in [450, 550]m$

(c) 3D examples for $z \in [400, 600]m$

Figure 9: The results of outflow-accumulation relationships in “+” type scenario.

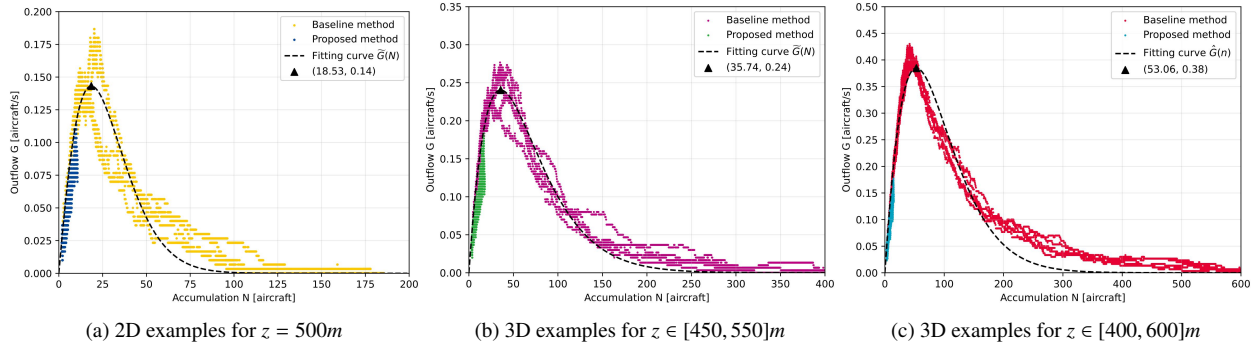


(a) 2D examples for $z = 500m$

(b) 3D examples for $z \in [450, 550]m$

(c) 3D examples for $z \in [400, 600]m$

Figure 10: The results of outflow-accumulation relationships in the “#” type scenario.

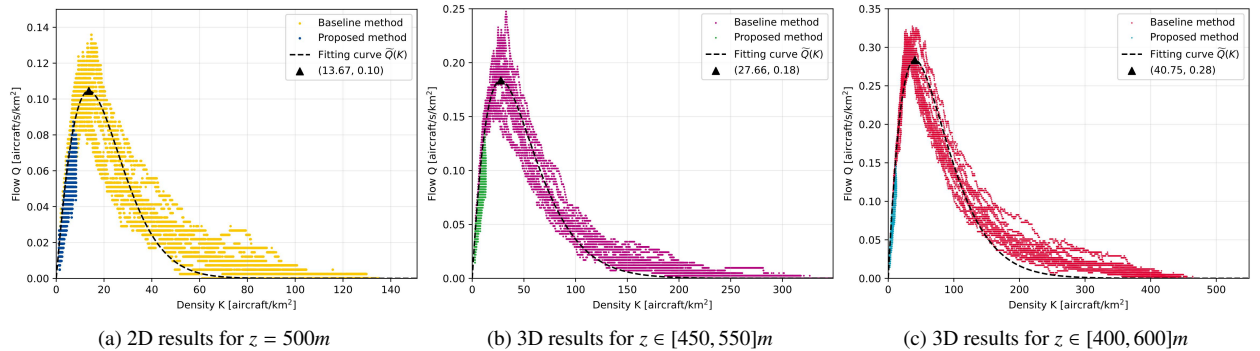


(a) 2D examples for $z = 500m$

(b) 3D examples for $z \in [450, 550]m$

(c) 3D examples for $z \in [400, 600]m$

Figure 11: The results of outflow-accumulation relationships in the “*” type scenario.



(a) 2D results for $z = 500m$

(b) 3D results for $z \in [450, 550]m$

(c) 3D results for $z \in [400, 600]m$

Figure 12: The results of flow-density relationships.

Under the demand setting illustrated in Figure 7, the proposed framework exhibits obvious advantages compared to the baseline, due to the detrimental effects of traffic congestion on network performance. To provide a comprehensive comparison, we further evaluate the performance of the proposed framework and the baseline in uncongested cases. We modify the demand to a fixed level close to the critical flow and repeat the previous tests. The metrics of computational efficiency, average travel speed, and trip completion rate are selected for evaluation. The results are summarized in Table 3. Compared to the baseline, the proposed framework has considerable improvements in computational efficiency (433%), average travel speed (70.2%), and trip completion rate (130%). Besides, the improvement in computational efficiency is observed to be more pronounced as the simulation scale increases. Interestingly, the proposed framework requires additional computation for path planning but achieves higher overall efficiency. On the one hand, appropriate aircraft routes provided by path planning simplify the permitted velocity constraints (4), significantly reducing the computation required for collision avoidance. On the other hand, the fast approximation method for path planning in Section 2.2 is computationally efficient.

Table 3: Performance comparison of air traffic evolution.†

	Computational efficiency [iteration/s]				Average Travel Speed [m/s]				Trip Completion Rate [trip/s]			
	“+”	“#”	“*”	Mean	“+”	“#”	“*”	Mean	“+”	“#”	“*”	Mean
Baseline method	1.08	0.80	0.84	0.91	12.13	10.60	11.43	11.39	0.083	0.087	0.080	0.083
Proposed method	4.97	4.81	4.76	4.85	18.91	19.61	19.66	19.39	0.197	0.190	0.187	0.191

† For performance metrics, higher is preferable.

We conduct experiments to evaluate the performance of the proposed path planning method and summarize the results in Figure 13. As the problem scale increases, the computational time required for the fast method grows very slowly. In contrast, the computational time required for the optimal solution (obtained through exhaustive search) increases exponentially. The fast method is better suited for real-time simulation, as its computational time is less than the simulation period of $\Delta t = 1$ s. Note that the simulation in this paper is deployed on a PC. With a high-performance computing cluster, our framework can be implemented to solve large-scale UAM problems (far more than 250 aircraft). More importantly, the approximate solution provided by the fast method performs well, as it is very close to the optimal solution. As illustrated in Figure 14a-Figure 14b, the difference between the two solutions involves only one aircraft (with its path marked by a bold purple line) at a problem scale of ten aircraft. Additionally, the disparity in total time spent between the two solutions is less than 1.5%. The performance of the approximate solution demonstrates the great potential of the proposed framework in large-scale UAM simulation and management.

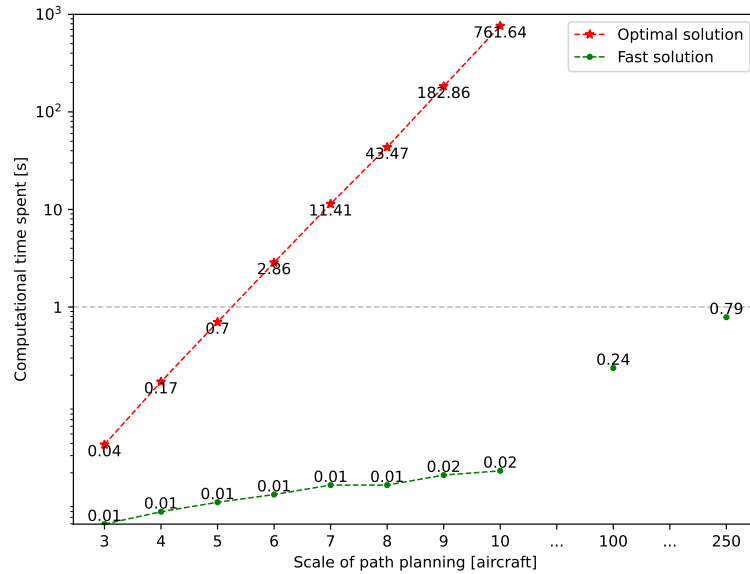


Figure 13: The computational time required by the exhaustive search and the fast approximation method.

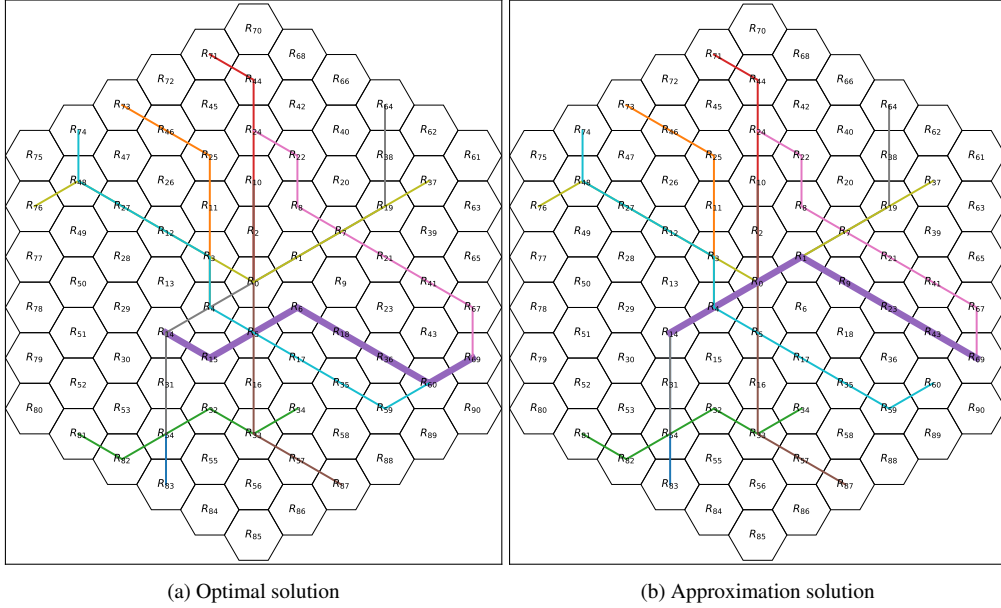


Figure 14: Comparison of the approximation solution and the optimal solution: the difference between the two solutions involves only one aircraft (with its path marked by a bold purple line).

Lastly, our proposed framework can also support flexible UAM operations for airspace management. Under the route guidance mechanism discussed in Section 2.2, a decrease in airspace region capacity n_l^{CR} would restrict aircraft from entering that region. By setting a small capacity for a specific region, we can reduce the number of aircraft entering that region. If necessary, we can clear the airspace for specific regions. An example of airspace clearance is illustrated in Figure 15. The clearance in airspace region R_0, R_1 and R_4 is dynamic for $t \in [2400, 3000]s$, with tiny external impacts. Dynamic airspace access management is crucial for various applications, including no-fly zones, privacy protection, and emergency response.

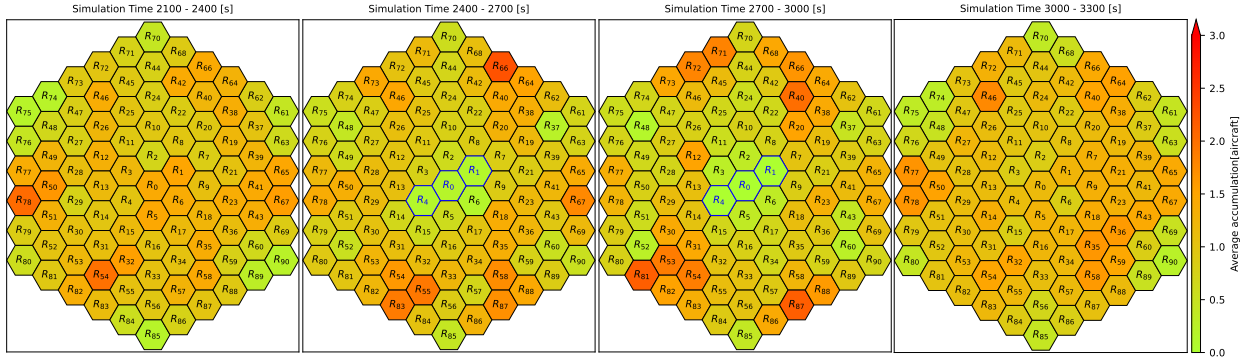


Figure 15: Dynamic airspace access management via capacity regulation: the airspace clearance of regions R_0, R_1, R_4 in $t \in [2400, 3000]s$ is generated for emergencies.

4. Conclusion

This paper focused on real-time traffic simulation and management for large-scale urban air mobility (UAM). Given that UAM is likely to be deployed between specific urban areas, dense point-to-point operations could increase the risk of aircraft collisions and air traffic congestion, particularly at large conflict points similar to roadway junctions. To address this, we proposed an operational framework that integrates route guidance and collision avoidance

for UAM aircraft. The proposed route guidance strategy provided aircraft with time-efficient paths composed of waypoints, while the collision avoidance algorithm generated safe trajectories between those waypoints. The proposed framework achieved great efficiency in large-scale UAM operations and retained an elegant property of the Macroscopic Fundamental Diagram (MFD) for air traffic upon guaranteeing air traffic safety.

To the best of our knowledge, this work is one of the first to combine route guidance and collision avoidance for UAM. By introducing the route guidance mechanism, aircraft are appropriately assigned across both spatial and temporal dimensions, which ensures air traffic homogeneity even for spatially heterogeneous demand. The simulation results demonstrated our framework's capability to guarantee the critical assumption of traffic homogeneity in the MFD model for air traffic (Geroliminis and Sun, 2011; Safadi et al., 2023a). Moreover, the results indicated that the proposed framework could enable efficient and flexible UAM operations, such as air traffic assignment, congestion prevention, and dynamic airspace clearance. Compared to the management scheme based on air corridors, the proposed framework achieved considerable improvements in computational efficiency (433%), average travel speed (70.2%), and trip completion rate (130%). The high computational efficiency implied the great potential of the proposed framework in large-scale UAM simulation and management.

The proposed framework can be easily transferred to multi-agent systems. Noting that this work has addressed route guidance in a compromised way, further studies in multi-agent path planning with the consideration of traffic congestion (or local deadlocks) would be a promising direction (e.g., Dergachev and Yakovlev, 2021). Back to the field of UAM, interesting directions for future work would include (i) investigating how to achieve macroscopic traffic flow control through microscopic aircraft control, e.g., by route guidance or speed limit; and (ii) developing adaptive and dynamic region division methods for route guidance.

Acknowledgement

The work in this paper was jointly supported by research grants from the National Natural Science Foundation of China (No. 72071214 & 62203239).

References

- Alrifae, B., Mamaghani, M.G., Abel, D., 2014. Centralized non-convex model predictive control for cooperative collision avoidance of networked vehicles, in: 2014 IEEE international symposium on intelligent control (ISIC), IEEE, pp. 1583–1588.
- Bahabry, A., Wan, X., Ghazzai, H., Menouar, H., Vesonder, G., Massoud, Y., 2019. Low-altitude navigation for multi-rotor drones in urban areas. *IEEE Access* 7, 87716–87731.
- Bauranov, A., Rakas, J., 2021. Designing airspace for urban air mobility: A review of concepts and approaches. *Progress in Aerospace Sciences* 125, 100726.
- Bradford, S., 2020. Urban air mobility (uam) concept of operations. Federal Aviation Administration. .
- Chen, C., Geroliminis, N., Zhong, R., 2024. An iterative adaptive dynamic programming approach for macroscopic fundamental diagram-based perimeter control and route guidance. *Transportation Science* 58, 896–918.
- Cummings, C., Mahmassani, H., 2024a. Airspace congestion, flow relations, and 4-d fundamental diagrams for advanced urban air mobility. *Transportation Research Part C: Emerging Technologies* 159, 104467.
- Cummings, C., Mahmassani, H., 2024b. Comparing urban air mobility network airspaces: Experiments and insights. *Transportation Research Record* 2678, 440–454.
- Dergachev, S., Yakovlev, K., 2021. Distributed multi-agent navigation based on reciprocal collision avoidance and locally confined multi-agent path finding, in: 2021 IEEE 17th International Conference on Automation Science and Engineering (CASE), IEEE, pp. 1489–1494.
- Dietrich, A., Wulff, Y., 2020. Urban air mobility: Adding the third dimension to urban and regional transportation, in: Presentation for: An Introduction to Urban Air Mobility for State and Local Decision Makers: A Virtual Workshop, sponsored by the Community Air Mobility Initiative (CAMI). Available online at <https://www.communityairmobility.org/uam101>.
- Garrow, L.A., German, B.J., Leonard, C.E., et al., 2021. Urban air mobility: A comprehensive review and comparative analysis with autonomous and electric ground transportation for informing future research. *Transportation Research Part C: Emerging Technologies* 132, 103377.
- Geroliminis, N., Sun, J., 2011. Properties of a well-defined macroscopic fundamental diagram for urban traffic. *Transportation Research Part B: Methodological* 45, 605–617.
- Haddad, J., Mirkin, B., Assor, K., et al., 2021. Traffic flow modeling and feedback control for future low-altitude air city transport: An mfd-based approach. *Transportation Research Part C: Emerging Technologies* 133, 103380.
- Han, R., Chen, S., Wang, S., Zhang, Z., Gao, R., Hao, Q., Pan, J., 2022. Reinforcement learned distributed multi-robot navigation with reciprocal velocity obstacle shaped rewards. *IEEE Robotics and Automation Letters* 7, 5896–5903.
- Holden, J., 2018. Uber keynote: Scaling uber air. Uber Elevate Summit, Los Angeles, CA, May 8.
- Huang, S., Teo, R.S.H., Tan, K.K., 2019. Collision avoidance of multi unmanned aerial vehicles: A review. *Annual Reviews in Control* 48, 147–164.

- Jang, D.S., Ippolito, C.A., Sankararaman, S., Stepanyan, V., 2017. Concepts of airspace structures and system analysis for UAS traffic flows for urban areas, in: AIAA Information Systems-AIAA Infotech@ Aerospace, p. 0449.
- Jose, K., Pratihari, D.K., 2016. Task allocation and collision-free path planning of centralized multi-robots system for industrial plant inspection using heuristic methods. *Robotics and Autonomous Systems* 80, 34–42.
- Kasliwal, A., Furbush, N.J., Gawron, J.H., McBride, J.R., Wallington, T.J., De Kleine, R.D., Kim, H.C., Keoleian, G.A., 2019. Role of flying cars in sustainable mobility. *Nature communications* 10, 1555.
- Kopardekar, P., Rios, J., Prevot, T., Johnson, M., Jung, J., Robinson, J.E., 2016. Unmanned aircraft system traffic management (UTM) concept of operations, in: AIAA Aviation and Aeronautics Forum (Aviation 2016).
- Li, Y., Ramezani, M., 2022. Quasi revenue-neutral congestion pricing in cities: Crediting drivers to avoid city centers. *Transportation Research Part C: Emerging Technologies* 145, 103932.
- Long, P., Liu, W., Pan, J., 2017. Deep-learned collision avoidance policy for distributed multiagent navigation. *IEEE Robotics and Automation Letters* 2, 656–663.
- Quan, Q., Fu, R., Cai, K.Y., 2021. Practical control for multicopters to avoid non-cooperative moving obstacles. *IEEE Transactions on Intelligent Transportation Systems* 23, 10839–10857.
- Safadi, Y., Fu, R., Quan, Q., Haddad, J., 2023a. Macroscopic fundamental diagrams for low-altitude air city transport. *Transportation Research Part C: Emerging Technologies* 152, 104141.
- Safadi, Y., Geroliminis, N., Haddad, J., 2024. Integrated departure and boundary control for low-altitude air city transport systems. *Transportation Research Part B: Methodological* , 103020.
- Safadi, Y., Geroliminis, N., Haddad, J., et al., 2023b. Aircraft departures management for low altitude air city transport based on macroscopic fundamental diagram, in: 2023 American Control Conference (ACC), IEEE. pp. 4393–4398.
- SESAR Joint Undertaking, 2017. U-space: Blueprint. Available at: <https://www.sesarju.eu/sites/default/files/documents/reports/U-space%20Blueprint%20brochure%20final.PDF>.
- Shen, X., Li, S., Li, M., Tang, Y., Chen, F., Sun, J., Xu, C., 2023. Low altitude economy development white paper (2.0) all digital solutions. Available at: <https://doc.weixin.qq.com/forms/ALIAUwdzAA8AMcA4wb7ABYUzKzwpn8Txf>.
- Shrestha, R., Oh, I., Kim, S., et al., 2021. A survey on operation concept, advancements, and challenging issues of urban air traffic management. *Frontiers in Future Transportation* 2, 626935.
- Sunil, E., Hoekstra, J., Ellerbroek, J., Bussink, F., Nieuwenhuisen, D., Vidosavljevic, A., Kern, S., 2015. Metropolis: Relating airspace structure and capacity for extreme traffic densities, in: ATM seminar 2015, 11th USA/EUROPE Air Traffic Management R&D Seminar.
- Tang, H., Zhang, Y., Mohmoodian, V., Charkgard, H., 2021. Automated flight planning of high-density urban air mobility. *Transportation Research Part C: Emerging Technologies* 131, 103324.
- Van Den Berg, J., Guy, S.J., Lin, M., Manocha, D., 2011. Reciprocal n-body collision avoidance, in: *Robotics Research: The 14th International Symposium ISRR*, Springer. pp. 3–19.
- Wang, H., Li, J., Chen, Q.Y., Ni, D., 2011. Logistic modeling of the equilibrium speed–density relationship. *Transportation Research Part A: Policy and Practice* 45, 554–566.
- Wu, Z., Zhang, Y., 2021. Integrated network design and demand forecast for on-demand urban air mobility. *Engineering* 7, 473–487.
- Xue, M., Do, M., 2019. Scenario complexity for unmanned aircraft system traffic, in: AIAA Aviation 2019 Forum, p. 3513.
- Yang, X., Wei, P., 2020. Scalable multi-agent computational guidance with separation assurance for autonomous urban air mobility. *Journal of Guidance, Control, and Dynamics* 43, 1473–1486.
- Yasin, J.N., Mohamed, S.A., Haghbayan, M.H., Heikkonen, J., Tenhunen, H., Plosila, J., 2020. Unmanned aerial vehicles (uavs): Collision avoidance systems and approaches. *IEEE access* 8, 105139–105155.